The Heart Surgery Forum 2022-4919
25 (5), 2022 [Epub September 2022]
doi: 10.1532/hsf.4919

Online address: http://journal.hsforum.com

M2 Macrophage-Derived Exosomes Regulate Myocardial Ischemia-Reperfusion And Pyroptosis Via ROS/NLRP3 Pathway

Hui Hu, MM,[1,2] Lei Qi, MS,[3] Changjie Ren, MM,[2] Suhua Yan, MD[1]

[1]Department of Cardiology, Shandong Provincial Qianfoshan Hospital, Cheeloo College of Medicine, Shandong University, Jinan, Shandong Province, China; [2]Department of Cardiology, Jining No.1 People's Hospital, Jining, Shandong Province, China, [3]Shandong First Medical University & Shandong Academy of Medical Sciences, Jinan, Shandong Province, China

ABSTRACT

Objective: To evaluate whether M2 macrophage-derived exosomes protect against MI/R injury and reveal the protective mechanism of exosomes [Kourembanas 2015].

Methods: I/R model injury was induced by temporary left anterior descending coronary artery occlusion in Sprague-Dawley (SD) rats, macrophages isolated from bone marrow-derived macrophages (BMDMs) were induced to M2 polarization, and H9C2 cells subjected to hypoxia/reperfusion (H/R) were used to establish an in vitro model. I/R-induced rats and H/R-induced H9C2 cells were treated with M2-exos in vivo and in vitro, respectively. Masson staining was performed to observe myocardial fibrosis in rats. Immunohistochemical (IHC) staining of myocardial tissues showed the expression of NLRP3 inflammasome activation and pyrolysis. Exosomes derived from IL-4-treated macrophages (M2-exos) were detected by transmission electron microscopy (TEM), nanoparticle tracking analysis (NTA) and western bolt. Western bolt was performed to determine the protein level, including NLRP3, pro-caspase-1, cleaved caspase-1, pro-IL-1β, cleaved IL-1β, gasdermin D (GSDMD), and N-terminus of gasdermin D (GSDMD-N).

Results: Activity of NLRP3 inflammasome and existence of pyroptosis in the rats subjected to MI/R were significantly higher than those in the control ($P < 0.05$). Moreover, we confirmed the accumulation of ROS during I/R injury in cardiomyocytes. M2-exos protected against I/R injury and reduced activity of NLRP3 inflammasome and existence of pyroptosis, accompanied with attenuating oxidative stress. In vitro studies showed similar effects, H9c2 cells co-cultured with M2-exos could attenuated H/R-induced cell injury, while M2-exos suppressed the expression of NLRP3 inflammasome and pyroptosis ($P < 0.05$).

Conclusion: MI/R leads to NLRP3 inflammasome and pyroptosis. M2-exos protect against I/R injury in a NLRP3-GSDMD-dependent manner.

INTRODUCTION

Acute myocardial infarction (AMI) is one of the leading global causes of morbidity and mortality [Anderson 2017]. Restoration of perfusion, including thrombolytic therapy, percutaneous coronary intervention (PCI) and coronary artery bypass graft (CABG) surgery after AMI, is the most frequent and effective medical treatment, but the process may inflict massive ischemia/reperfusion (I/R) injury [Merz 2019]. I/R injury can induce the death of cardiac fibrosis or even cardiomyocytes and is estimated to occur in up to 60% of patients [Moon 2020]. The pathogenesis of MI/R, which involves many signaling pathways, is multi-faceted and complicated, including oxidative stress, pyroptosis, and proinflammatory programmed cell death. An effective alternative therapy urgently is required for the reperfusion period and the development of new treatment for attenuating oxidative stress, mitigation of an inflammatory response, and alleviating cellular damage.

Macrophages, as central players of the inflammatory response in the heart, play an important role on repair and remodeling of the infarcted heart by regulating the delicate balance between pro-inflammatory reactions and the suppression of inflammation [Frangogiannis 2015; van der Vorst 2019; Jung 2018]. As a key component of innate immunity, macrophages can be detected in the heart microenvironment time after infarction. According to their polarization state, macrophages are categorized into two main subtypes: classically activated macrophages (M1), also referred to as 'killer' macrophages, and alternatively activated macrophages (M2), also referred to as "repair" macrophage [Grivennikov 2010; Sica 2008]. It is well known that M2 macrophages mediate the resolution of inflammation and promote injured tissue repair/remodeling [Cheng 2018; Ma 2018; Martinez 2014]. As effective functioning of macrophages in a cardiac microenvironment could be the result of interactions between macrophages and other types of immune cells as well as additional cell types, there is an urgent need to conduct a more in-depth exploration of interaction network construction.

Received June 6, 2022; received in revised form June 27, 2022; accepted June 28, 2022.

Correspondence: Suhua Yan, Department of Cardiology, Shandong Qianfoshan Hospital, Cheeloo College of Medicine, Shandong University, No. 16766 Jingshi Road, Jinan 250014, Shandong Province, China, Telephone 86-531-89269418, Fax 86-531-82963647 (e-mail: yan_suhua5487@21cn.com).

Exosomes are small membrane vesicles, ranging from 30-150 nm ubiquitously present in nearly all body fluid [Zhang 2019; Xu 2018]. Exosomes transfer plenty of types of nucleic acids and proteins to recipient cell as mediators of intercellular communication [Denzer 2000]. Previous study has reported that exosomes play a critical role in cardioprotection, including the regeneration and reconstruction of blood vessels and alleviation of the inflammatory response [Teng 2015]. Recent studies have revealed that macrophages -derived exosomes constitute a large proportion of circulating microvesicles in blood [McDonald 2014], which involved in the progression in various diseases [Xiong 2020]. So far, however, there has been little discussion about whether M2-exos have an effect on repair and remodeling of the infarcted heart following I/R.

Recent studies have revealed that NLRP3-related pyroptosis plays an important role in MI/R injury [An 2019]. Accumulation of NLRP3 inflammasomes always has been considered an important catalyst for pyroptosis. I/R can result in the activation of NLRP3 inflammasome, briefly, NOD-like receptors located in the cytoplasm can recruit pro-Caspase-1 in the cell directly or through ASC to form a multi-protein complex. As the local concentration of pro-Caspase-1 is elevated, self-shearing occurs to generate activated Caspase-1, which in turn cleaves the Gasdermin D into GSDMD N terminus [Liu 2016; Shi 2014]. The gasdermin pores, formed by the previously cleaved GSDMD N terminus, lead to release of mature IL-1β which results in cell membrane swelling, rupture and typically a type of necrotic cell death [Ding 2016]; this process is defined as pyroptosis classical activation. Pyroptosis, newly discovered pattern of programmed cell death, occurs in a variety of tissues. Moreover, pyroptosis not only leads to cell death, but it also induces excessive inflammatory damage [Wang 2021]. However, whether M2-exos protect against MI/R injury in a NLRP3-GSDMD-dependent manner remains largely understudied.

In the present study, we demonstrated the existence of NLRP3 inflammasomes and pyroptosis during MI/R injury. Additionally, the aim of this study was to reveal the protective effect of M2-exos that occurs during MI/R injury and to elucidate the underlying mechanism.

MATERIALS AND METHODS

Animals and experimental groups: Experiments were performed on 8-week-old Sprague-Dawley rats (240-250 g; Vitalriver Co.; Beijing, China). The rats were raised in an animal facility at a constant temperature of 25±5°C and relative humidity of 70%±20% with a 12 h light/dark cycle. All animal procedures undertaken in this study were strictly according to the Animal Care Committee of the Shandong Qianfoshan Hospital, Cheeloo College of Medicine, Shandong University. Rats were acclimatized for 7 days in their new environment before initiation of the experiment.

The rat MI/R model was established as previously described [Xue 2016; Liu 2013]. In short, all rats were anesthetized with intraperitoneal 3% 1 ml/kg pentobarbital sodium after weighed individually, and then mechanically ventilated with a rodent ventilator (RWD Life Science, Shenzhen, China). Subcutaneous needle electrodes were placed and electrocardiogram (ECG) was continuously monitored and recorded during the experiment. Following the skin incision, the heart was exposed after pericardiotomy through a left-sided thoracotomy in the fourth intercostal space. MI/R model was induced by ligation of the left anterior descending coronary artery (LAD) for 30 min and then reperfused for 2 h. The control groups were subjected to the same procedures but without LAD ligation.

The successful establishment of myocardial ischemia are as follows: An ischemic ECG was defined as a widened QRS complex, elevation of the ST segment, height and pointed of T wave, as well as the apical and anterior wall of the left ventricle (LV) turned pale with abnormalities in regional ventricular wall motion. The successful reperfusion of myocardial ischemia is defined as the color changing from pale to red in the apex and anterior wall of the left ventricle, and ECG showing a ventricular arrhythmia and a decline in ST-segment.

In vivo experiment, to verify whether exosomes can be absorbed by myocardial tissues, exosomes were labeled with DiR dye and injected into rats via the tail vein. The rats in the control group were injected with an equal amount of PBS. Myocardial tissues were removed, and DiR dye signals were quantified after injection, then, images were observed by fluorescence microscopy.

Experimental design – Three independent experiments were performed

Protocol 1: M2 polarization of primary macrophages isolated from bone marrow of SD rats via IL-4 treatment, which immunophenotypic characterization was performed by flow cytometry and qRT-PCR. Exosomes isolated from M2 macrophages identified using TEM, NTA and Western blotting assay.

Protocol 2: Exosomes were utilized for vivo experiments. N rats were randomized into the following four groups (N = 30 in each): control, MI, MI+PBS, and MI+exos. MI models were established as previously described. Experiments were designed to evaluate activation of NLRP3 inflammasome and pyroptosis of myocardial tissues. The plasma and heart tissues were collected and used for Western blotting, immunohistochemistry, immunofluorescent and ELISA.

Protocol 3: Exosomes were utilized for vitro experiments. Cell lines were randomly divided into 4 groups: control group, MI group, MI+PBS, MI+exos. Cells were subjected to establishment of hypoxia-reoxygenation model. In this protocol, CCK-8 assay, TUNEL assay, Caspase-1 activity assay, LDH release assay, immunofluorescent, Western blot and qRT-PCR were performed.

BMDMs preparation and polarization: We obtained BMDMs from bone marrow cells from the femur and tibia of SD rats. The primary macrophages cells were resuspended in RPMI medium supplemented with 10% heat-inactivated fetal bovine serum (FBS, Invitrogen, Carlsbad, CA, USA), 1%(v/v) penicillin/streptomycin (Gibco, Thermo Fisher Scientific,

Inc.). To induce the polarization of macrophages, macrophages were treated with 20 ng/mL of IL-4 (Rocky Hill, NJ, USA). After the 24 h polarization, the supernatant was collected for further analysis.

Cell culture and Hypoxia-Reoxygenation Model (H/R): H9c2 embryonic rat cardioblastic cells, purchased from Wuhan Pu-nuo-sai Life Technology Co. Ltd. (Wuhan, China), were incubated in DMEM (Invitrogen, Thermo Fisher Scientific, Inc.) filled with 10% FBS, 1%(v/v) penicillin/streptomycin and 2mM glutamine in an atmosphere with 5% CO2 at 37°C. H9c2 cells were exposed to H/R to mimic an ischemic-like microenvironment in vitro. H9c2 cells were cultured in serum-free and glucose-free medium, incubated at 37°C in an anaerobic glove box (MBRAUN, Garching, Germany) gassed with 95% N2 and 5% CO2 at 37°C lasted for 6 h. Then H9c2 cells were removed to the regular incubator with the medium replaced by fresh complete culture medium for 12 h to simulated reperfusion.

Isolation and identification of cellular exosomes: Exosomes were isolated from 500 µL of plasma using the exoEasy Maxi Kit (Qiagen, Hilden, Germany), following the manufacturer's instructions. Briefly, plasma samples were used pre-filtered with 0.8-µm filter to remove cells and cell debris, followed by mixing with the same volume of XBP buffer, the mixture was added to the exoEasy centrifugal column and centrifuged. The bound exosomes were washed with XWP buffer through a centrifuged, then was eluted used XE buffer. Final exosomes were dissolved in PBS and stored at –80°C until analysis. Transmission electron microscopy (TEM, Hitachi HT-7800, Japan), nanoparticle tracking analysis (NTA, NanoSight, Amesbury, UK) were used to observe the isolated exosomes. The expression of the typical exosomal markers CD63, TSG101 was detected by Western blot.

Exosome uptake assay: Exosomal suspension and PKH67 dye diluted 1:1000 was mixed and incubated at 37°C for 15 min and protected from light. The PKH67-labeled exosomes preparation was completed after ultracentrifugation at 120,000xg for 70 min. The PKH67-labeled exosomes were cocultured with H9c2 cells for 30 min after being washed with PBS. Treated H9C2 cells were fixed using 4% paraformaldehyde for 15 min, nuclei were counterstained with DAPI (1:500, Invitrogen, Carlsbad, CA, USA). Images were acquired using confocal microscopy at 6 h, 12h and 24 h.

Masson trichrome staining and infarct size measurements: Masson's trichrome staining was performed with the Masson Stain Kit (Nanjing Jiancheng Bioengineering Institute, Nanjing, China) following standard protocols. Hearts were removed from the chest cavity and sliced into 3 transverse sections along the top and bottom edges of the infarction. The mesial-most myocardial tissues were fixed in 10% formalin for 24 hours and processed in paraffin and embedded. The sections were cut into 10µm appropriate thickness followed by Masson trichrome staining. Infarct size (%) was calculated as mean percentage of the endocardial+ epicardial circumferences of infarcted area versus the total endocardial+ epicardial circumferences of LV.

Immunohistochemistry: Apical halves from partially resected LV were collected and washed in PBS for immunohistochemistry analysis. Tissue samples were fixed in 10% formaldehyde, dehydrated, and embedded in paraffin. The sections were cut into 5 µm then incubated with the primary antibodies for NLRP3 antibody (1:100; CST, USA), Caspase-1 antibody (1:100; NOVUS, USA), IL-1β antibody (1:100; Abcam, USA), and GSDMD antibody (1:100; Abcam, USA) overnight at 4°C. After three washes with PBS, tissue samples were incubated with secondary antibody for a horseradish peroxidase-labeled anti-rabbit/mouse IgG (1:1000, Sigma Aldrich, USA) for 2 hours. The tissue samples were observed using a microscope (IX71, Olympus, Tokyo, Japan), and five visual fields were randomly taken for taking photos, the results of which were determined with ImageJ analysis software (MediaCybernetics, Inc., Bethesda, MD, USA). The average percentage of positive cells in each specimen was obtained from five random visual fields.

Determination of reactive oxygen species (ROS): The ROS in myocardial tissues level were performed by the dihydroethidium (D11347, Thermo Fisher Scientific, Waltham, MA, USA) staining following the manufacturer's instructions. After collection, tissues were rinsed in cold (4°C) PBS and frozen in embedded in OCT (Tissue-Tek) at -80°C. The LV myocardium was cut into 10-µm-thick sections in a cryostat, which was incubated with 10µL of DHE probefor 30 min at 37°C in the dark. Fluorescence images were examined under a confocal microscope (BX53; Olympus Optical, Tokyo, Japan). The fluorescent density in the cardiomyocytes within five random optical sections was determined with ImageJ analysis software.

The intracellular ROS was measured using dichlorodihydro-fluorescein diacetate (DCFH-DA, Molecular Probes, Life Technologies, Invitrogen, Eugene, OR, USA), according to the manufacturer's protocol. The cells in each group were incubated in 5µM DCFH-DA at 37°C for 20 min. The intracellular ROS was captured by confocal microscope equipped with UltraVIEW VoX Confocal Imaging System (PerkinElmer, Wellesley, MA) at excitation wavelength of 485 nm and emission wavelength of 530 nm.

Flow cytometry: Stimulated cells were collected and incubated with rabbit anti-CD206 (ab64693, Abcam, USA) at 4°C for 30 min. After washing with PBS twice, cells were analyzed using flow cytometry (Beckman Coulter Cytoflex; Beckman, USA), then data were analyzed with FlowJo software (FlowJo, Ashland, OR, USA).

Cell viability assay: Cell viability assay was evaluated through Cell Counting Kit-8 (CCK-8). According to experimental setting, 3000 cells per well were seeded in 96 well plates and were incubated with 10 µl CCK8 solution for 2 hours at 37°C. The absorbance at 450 nm was detected with a microplate reader (Thermo Scientific, USA).

Measurement of lactate dehydrogenase (LDH) release: The LDH release was measured by the colorimetric assay, cells belonging to different experimental groups were seeded in 96-well plates, incubated at 37°C for 24 h. After centrifugation, 120 µl cell supernatant was added to a new 96-well plate added 60 µL of LDH detection work solution per well of a 96-well plate. The absorbance was read at 490 nm detected with a microplate fluorescence reader (Synergy

H1 microplate reader, BioTek, Winooski, VT, USA).

Caspase-1 Activity Assays: The activity of Caspase-1 from cell lysates was determined using a commercial Caspase-1 Activity Assay Kit (C1101, Beyotime Biotechnology, Shanghai, China). Cell lysates were incubated with 5 μL of acetyl-Tyr-Val-Ala-Asp p-nitroaniline (Ac-YVAD-pNA) at 37°C for 1h. The absorbance values of p-nitroaniline (pNA) were detected at a wavelength of 405 nm using a microplate reader, which was to assess the activity of the Caspase-1.

Biochemistry indicators measurement: After reperfusion, the arterial blood samples were collected. The level of serum creatine kinase-MB (CK-MB) was measured with CK-MB isoenzyme assay kits (Roche, Indianapolis, IN, USA) and serum LDH by LDH assay kit (Roche, Indianapolis, IN, USA), according to the manufacturer's instructions. The level of malondialdehyde (MDA), superoxide dismutase (SOD) was measured by enzyme-linked immunosorbent assay (ELISA), according to the manufacturer's instructions. The absorbance was measured using a microplate reader (Varioskan® Flash; Thermo Fisher Scientifc, Waltham, MA, USA).

Quantitative real-time PCR (qRT-PCR) detection: RNAs were extracted using TRIzol reagent (Invitrogen, CA, USA) from myocardial tissues. For reverse transcription, a PrimeScript™ RT kit (Vazyme Biotech Co., Nanjing, China) was used. The following primers were used: GAPDH: forward 5' -GGTCGGAGTCAACGGATTTGGTCG-3',reverse5'-CCTCCGACGCCTGCTTCACCAC-3'; Arg1: forward5'-GGCAGAAGTCAAGAAGAACGGA-3',reverse5'-GTGAG-CATCCACCCAGATGA-3'; The 2-△△CT method was utilized for calculating the relative targeted gene expression.

Western blot analysis: The protein expression in myocardial tissues (N = 10) was assessed by Western blot as previously described [He 2018]. In short, RIPA lysis buffer was used to extract the total protein, then the proteins were transferred onto polyvinylidene difluoride (PVDF) membranes after being separated using sodium dodecyl sulfate-polyacrylamide gel electrophoresis (SDS-PAGE). The resulting blots were blocked with 8% skim milk and incubated with anti-NLRP3 antibody (1:1000; Cell Signaling Technology, USA), anti-Caspase1 antibody (1:1000; Proteintech, China), anti-IL-1β antibody (1:1000; Abcam, USA), anti-N-terminal of GSDMD (1:1000; Abcam, USA), anti-GAPDH rabbit monoclonal (1:1000; Cell Signaling Technology, USA) overnight at 4°C. Then, the membrane was incubated with horseradish peroxidase-conjugated secondary antibodies (1:10000; Abcam, USA) at room temperature for 2 h. Proteins were detected with using ECL chromogenic substrate (Millipore, MA, USA).

Statistical analysis: The measurement data are presented as mean ± standard deviation (SD). All statistical data were analyzed with the SPSS 22.0 (SPSS, Inc. Chicago, IL, USA). Two-tailed unpaired Student's t tests and one-way analysis of variance (ANOVA) were used for the comparison among

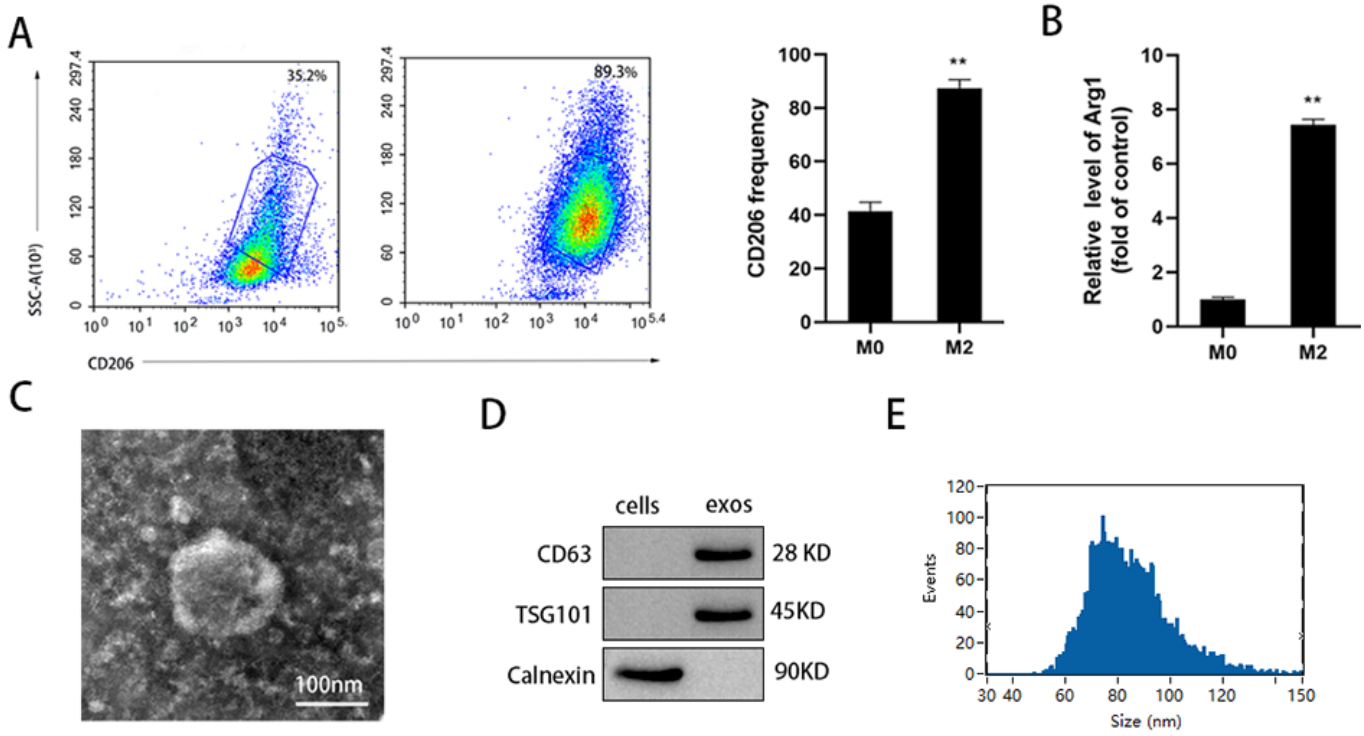

Figure 1. Isolation and identification of M2 macrophage-derived exosomes. A) Representative flow cytometry plots and summary data showing M2 macrophages using CD206 as the markers (N = 4 in each group). B) The relative mRNA expression of arginase 1 (Arg1) was evaluated by reverse-transcriptase polymerase chain reaction. C) Observation of exosome morphological characteristics by TEM (scale bar=100 nm). D) Western blot analysis of the expression of exosome markers (TSG101, CD63, Calenxin). E) detection of exosome diameter by Nano Sight particle-tracking analysis. The values are shown as mean ± SEM (N = 6). $^{**}P < 0.01$ vs. the M0 group; the experiment was repeated three times.

the two and three groups, respectively. The figure was made by GraphPad Prism 8.0 (GraphPad Software, USA). All tests were two-sided, and $P < 0.05$ was considered to be statistically different.

RESULTS

Identification of polarized BMDMs and exosomes: We cultured BMDMs from bone marrow precursor cells of SD rats with M-CSF, and then treated with LPS to obtain M2 phenotypes. Polarized M2 macrophages were confirmed by examining the expression of CD206, one of typical M2 surface marker, by using flow cytometry (Figure 1A), Western blot was performing to observe the expression production of arginase 1 (Arg1) (Figure 1B). (Figure 1)

After optimization of the exosome isolation from plasma, we verified the successful exosome harvesting through TEM, western blot of exosome markers, and NTA. TEM images were used to show the size and shape of particles of exosomes and revealed that the exosomes had circular-like, bilayer membrane vesicle structure (Figure 1C). Western blot analysis confirmed the low expression of non-exosomal marker Calnexin and high levels of specific exosomal membrane markers, CD63 and TSG1(Figure 1D). In order to detect the size range of cellular exosome diameters NTA was used, and it confirmed the average size of the exosomes to be 80-100nm (Figure 1E).

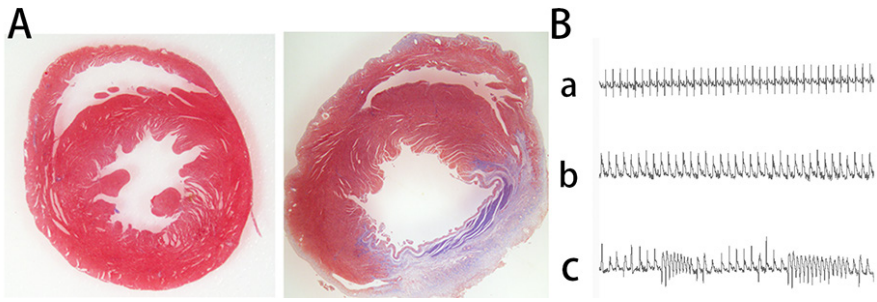

Figure 2. A rat model of myocardium ischemia-reperfusion was successfully generated. A) Masson's trichrome-stained myocardial infarcted sections at 3 days after MI in rats, red, myocardium; blue, scarred fibrosis. B) Corresponding ECG. The values are shown as the mean ± SEM ($N = 6$). The experiment was repeated three times

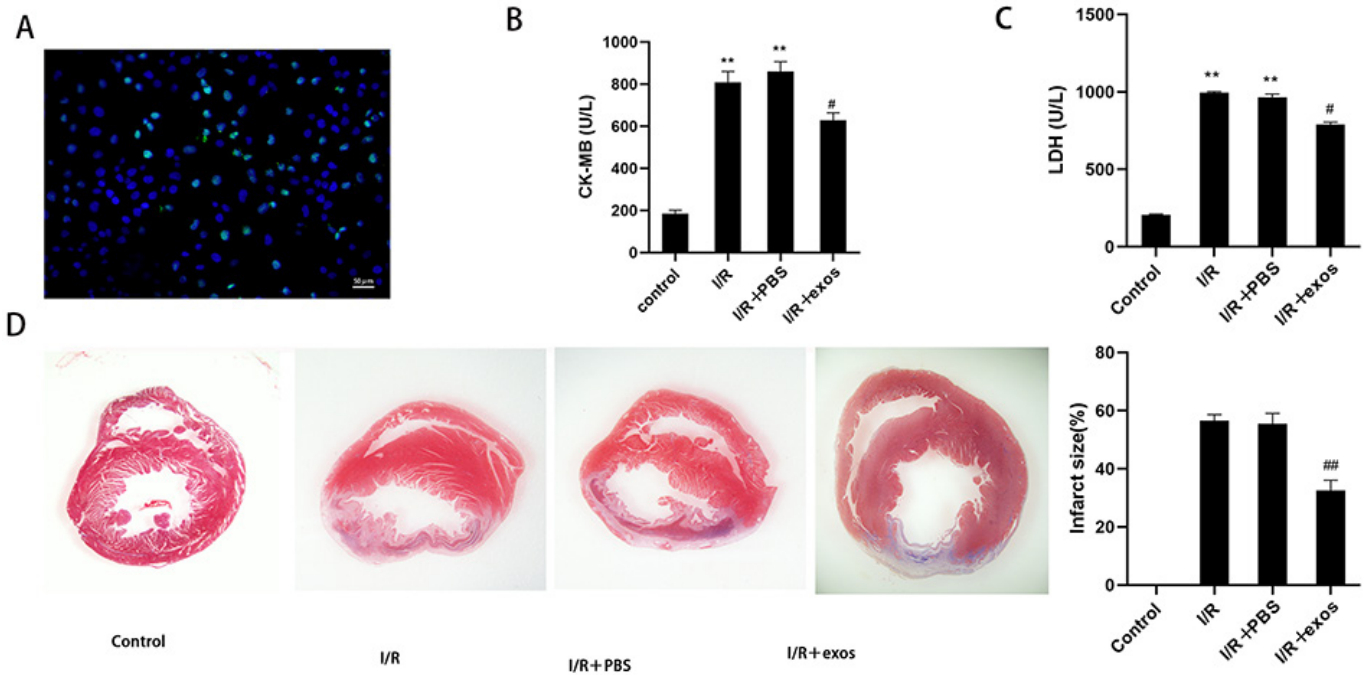

Figure 3. M2-exos protected against cell injury. A) Representative images of DIR-labeled exosomes from rats and DAPI-stained cardiomyocytes. The myocardial injury was evaluated with the serum CK-MB (B) and LDH (C) levels. D) Masson's trichrome-stained myocardial infarcted sections on the third day, following MI in rats. The values are shown as the mean ± SEM ($N = 6$). ***$P < 0.001$, **$P < 0.01$ compared with the control group; #$P < 0.05$ compared with I/R+PBS group. The experiment was repeated three times.

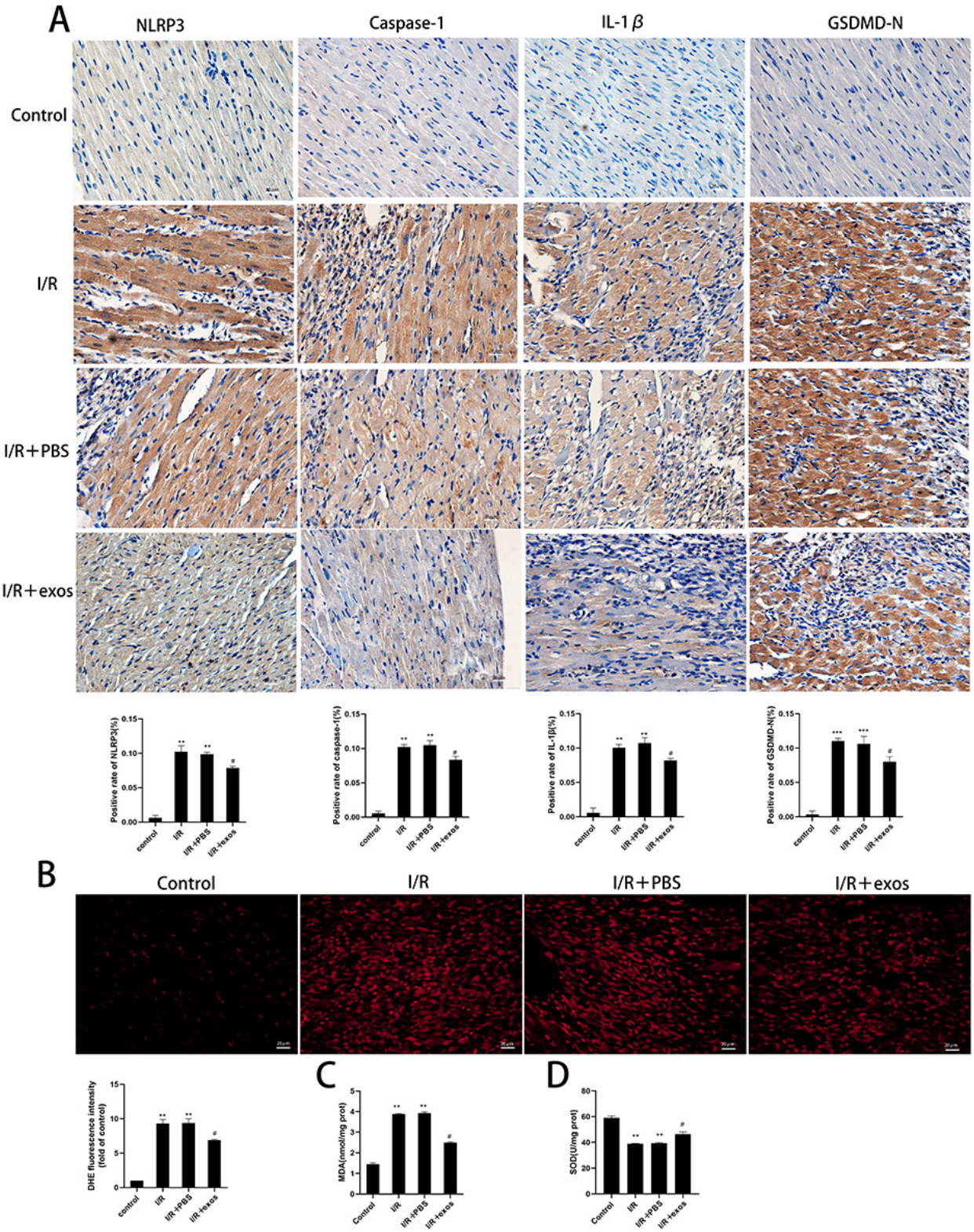

Figure 4. M2-exos induced activation of the NLRP3, pyroptosis and myocardial oxidative stress in vivo. A) IHC staining of the NLRP3 inflammasome and pyroptosis in myocardial tissues. B) ROS production was measured by DHE staining in fresh frozen section of left ventricle. The concentration of MDA (C) and SOD (D) in myocardial tissue were detected by ELISA. The values are shown as the mean ± SEM ($N = 6$). $^{**}P < 0.01$, $^{*}P < 0.05$ compared with control group. $^{\#}P < 0.05$ compared with I/R PBS group. The experiment was repeated three times.

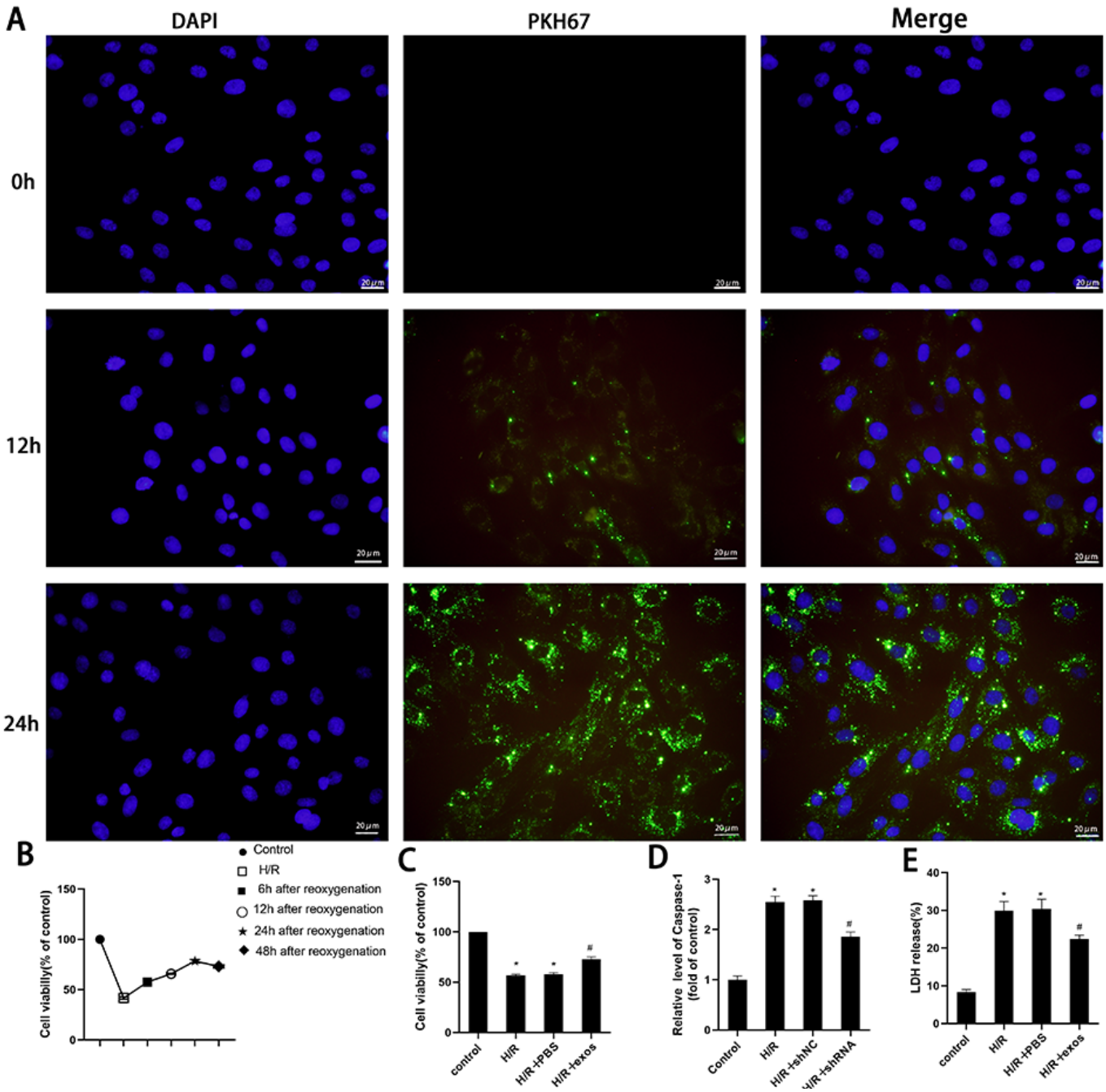

ischemia-reperfusion injury in vitro. A) Uptake of PKH-67-labelled M2-exos by H9C2 cells (scale bar=20 μm). B and C) Cell viability was measured with CCK-8 assay. D) Caspase-1 activity was measured. E) The releasing levels of LDH were detected. The values are shown as the mean ± SEM ($N = 6$). *$P < 0.05$ compared with the control group; #$P < 0.05$ compared with the H/R + PBS group. The experiment was repeated three times.

Model of MI/R injury in rats was established: Model of MI/R injury in rats was established for the next research. The successful performance of reperfusion was confirmed by inspection of color in the apical part of the left ventricle. Masson staining was utilized to observe the histopathological features of the myocardial tissue of rats with MI/R injury (Figure 2A). (Figure 2) Myocardial cells in the sham group were intact and arranged in order. However, in the I/R group, myocardial cells were disordered and swollen, myofibrils were contractured, and sarcolemma was disrupted. Typical ECG changes, including decline of the ST-segment and the occurrence of reperfusion-induced ventricular premature contractions (PVC) and ventricular tachycardia (V Tach) (Figure 2B), were performed. The data above showed that the model of

MI/R successfully was established.

M2-exos alleviated myocardial tissues injury after I/R injury: To determine the exosomes could uptake by cardiomyocyte, we treated the rats with the Diol-labeled (green) exosomes by tail vein injections before reperfusion and observed the frozen myocardial sections using immunofluorescence microscope. As shown in (Figure 3A), the green fluorescent markers were clustered around the blue nucleus in the myocardial tissue, which proved that M2-exos could access myocardial tissues through the systemic circulation. (Figure 3)

We verified that M2-exos protect against I/R-induced myocardial injury. The ELISA results demonstrated that the concentrations of CK-MB (Figure 3B) and LDH (Figure 3C) in serum were significantly increased in I/R group when compared with control group, while suppressed by M2-exos treatment. As shown in (Figure 3D), M2-exos reduced the myocardial infract size and significantly decreased the levels of CK-MB in rats subjected to MI/R injury. We affirmed that M2-exos suppress myocardial tissues injury in MI/R rats.

M2-exos suppresses I/R-induced NLRP3 inflammasome activation, pyroptosis and oxidative stress in vivo: Given GSDMD-N is the executor of pyroptosis, the cleavage of GSDMD is used as an index for assessing pyroptosis [Shi 2015]. To determine the presence of NLRP3 inflammasome activation and pyroptosis, myocardial specimens collected from MI/R injury model accessed by immunohistochemistry. As shown in Figure 4A, I/R-induced myocardial damage were associated to NLRP3 inflammasome activation and pyroptosis, which were evidenced by increased expression of NLRP3, enhanced cleavage of caspase-1, IL-1β, IL- 18 and GSDMD in the myocardial tissues compared with control. (Figure 4) It also is evident that the expression of NLRP3, Caspase-1, IL-1β and GSDMD in myocardial tissues were suppressed after M2-exos treatment. Given that ROS plays a central role in NLRP3 inflammasome activation [Abderrazak 2015], we observed the expression of ROS level by DHE staining. As shown in Figure 4B, rats were subjected to MI/R and exhibited significant increased level of the ROS in myocardial tissues compared with the control group, while decreased after M2-exos treatment. To estimate the effect of M2-exos on myocardial oxidative stress subject to I/R injury, we evaluated the levels of MDA and SOD in myocardial tissues, which were detected by ELISA. MDA (Figure 4C) and SOD (Figure 4D) were significantly increased in I/R group, while all were decreased by M2-exos treatment. To sum up, M2-exos treatment inhibited NLRP3 inflammasome activation, pyroptosis and myocardial oxidative stress after I/R injury.

M2-exos alleviated injury in H9c2 cells after H/R: To explore whether M2-exos could suppresses damage in H9c2 cells after H/R injury, we treated cells with M2-exos. Myocardial cell damage by H/R was confirmed by CCK-8 assay, caspase-1 activity and LDH release. To determine whether the exosomes could uptake by H9C2 cells, an exosome uptake assay was performed. By fluorescence microscopy, we found that PKH26-stained M2-exos could be gradually internalized by H9c2 cells only at 12 h and later (Figure 5A). (Figure 5) As shown in Figure 5B, the activation of cell viability peaked at 24h after stimulation. Therefore, 24 h was chosen as the optimal stimulation time in the next series of experiments. Myocardial cell damage by H/R was confirmed by CCK-8 assay, caspase-1 activity and LDH release. As an illustration, the H/R group showed significantly decreased cell viability compared with the control group. The activity of Caspase-1 (Figure 5D) and LDH release (Figure 5E) were significantly increased subject to H/R stimulation. However, M2-exos significantly increased cell viability by detecting CCK-8 assay, Caspase-1 activity and LDH release in H9C2 cells exposed to H/R insult. The above experimental results indicated the M2-exos increased cell activity in H9c2 cells after H/R.

M2-exos suppresses NLRP3 inflammasome activation, pyroptosis and oxidative stress in H9c2 cells after H/R: To evaluate whether M2-exos could suppress NLRP3 inflammasome activation and pyroptosis in H9c2 cells after H/R injury, we accessed NLRP3 inflammasome-related proteins by Western blots. As shown in Figure 6A, compared with the

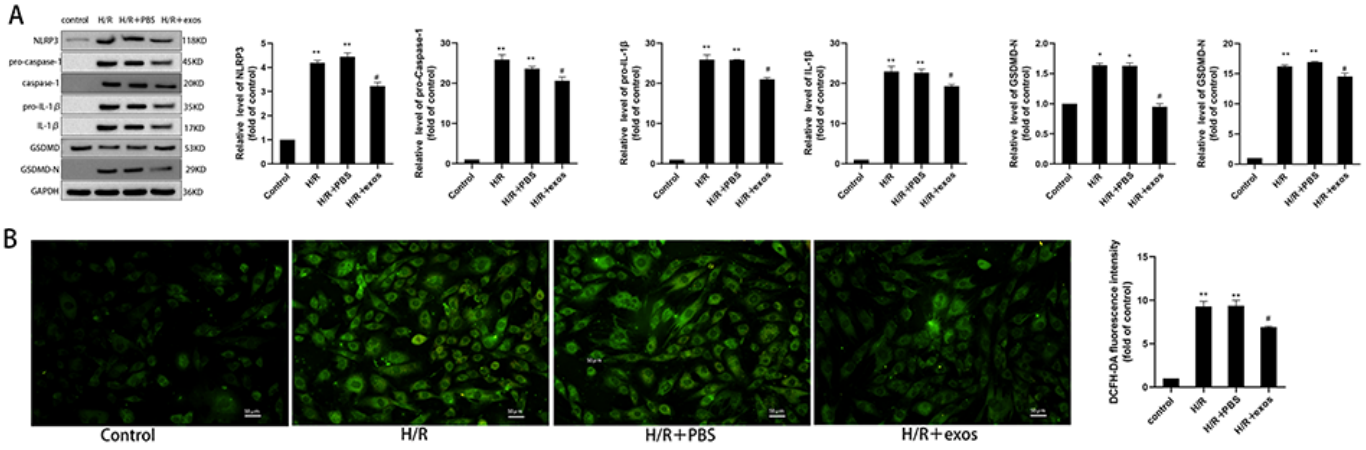

Figure 6. M2-exos protected H9c2 cells against H/R-induced NLRP3 inflammasome activation, pyroptosis and oxidative stress in vitro. A) NLRP3 inflammasome and pyroptosis-related proteins in H9c2 cells, were examined by Western blot. B) Intracellular ROS production was determined via DCFH-DA staining. The values are shown as the mean ± SEM (N = 6). The experiment was repeated three times.

control group, M2-exos significantly inhibited the expression of NLRP3, Caspase-1, IL-1β and GSDMD as executors of pyroptosis by Western blot. (Figure 6) We examined the changes in ROS in vitro and found that M2-exos suppresses the ROS. As shown in Figure 6B, results showed that the expression of NLRP3 and aggregation of ROS in H9c2 increased in H/R-treated cells, whereas were decreased subject to M2-exos treatment. The above experimental results indicated the M2-exos suppress NLRP3 inflammasome activation, pyroptosis, and oxidative stress in H9c2 cells after H/R.

M2-exos inhibit pyroptosis via the ROS/NLRP3 inflammasome pathway: The underlying mechanisms are unclear, and further investigations are required to expand on the current findings. Given that ROS plays a central role in NLRP3 inflammasome activation [Wrobel 2015], we sought to know whether H/R-induced NLRP3 inflammasome activation. The primary cardiomyocytes were pretreated with MCC950 (NLRP3 inflammasome inhibitor) for 1 hour before the H/R treatment. When cells were cultured in the presence of MCC950, the expression of GSDMD-N was observed by western blot (Figure 7A). (Figure 7) This result suggests that the inhibition of the NLRP3. Pretreatment with NAC for 1 hour reduced H/R-induced NLRP3 inflammasome expression (Figure 7B). All these findings suggest that M2-exos inhibited Inhibit pyroptosis via the ROS/NLRP3 inflammasome pathway.

DISCUSSION

Acute myocardial infarction was infrequent (0.8%) but resulted in a high death rate (42%) [Wrobel 2015]. On one hand, interventional therapy can improve the symptoms of myocardial infarction ischemia; on the other hand, subsequent reperfusion aggravates the damage in cardiomyocytes. MI/R injury is another piece of the puzzle in clinical practice, called 'hidden cardiotoxicity' [Ferdinandy 2019]. Many studies have focused on suppressing oxidative stress and inflammation to reduce I/R injury. It has been well-established that exosomes can carry lncRNA, miRNAs and proteins for intercellular communications, and exosomes form different sources that have been identified to reduce MI/R injury [Vicencio 2015; Chen 2013; Xiao 2017]. In the present study, the aim of the current study was to gain more insight into the mechanisms of M2 macrophages-derived exosomes in tissues and cells after ischemic and hypoxia reperfusion injury, with a conclusion that M2-exos could protect myocardial tissues via suppressing oxidative stress and inflammation to reduce I/R injury.

A notable finding of the present study is that we determined the presence of pyroptosis in MI/R injury and M2 macrophages-derived exosomes had a robust effect against pyroptosis. Pyroptosis is a caspase-1-dependent cell death first proposed as an active, novel form of programmed cell death [Bergsbaken 2009]. Pyroptosis is triggered by various stimuli and initiated by the activation of GSDM family proteins [Shi 2015]. In this study, we identified activation of NLRP3 inflammasome during I/R injury. More importantly, we found an increased level of N-terminus of GSDMD, suggesting the appearance of pyroptosis. It is clear from the results of our experiments that pyroptosis is a significant cause of cell death during I/R. In summary, we revealed the activation of NLRP3 inflammasomes and pyroptosis during I/R.

In general, the M1 macrophage phenotype is proinflammatory and can induce tissue destruction, whereas, the M2 macrophage phenotype accounts for anti-inflammatory attributes and are implicated in tissue regeneration, growth, and remodeling [Gaspar 2018]. M2 macrophage was shown to be have a remission on tissues and other organs I/R injury [Yue

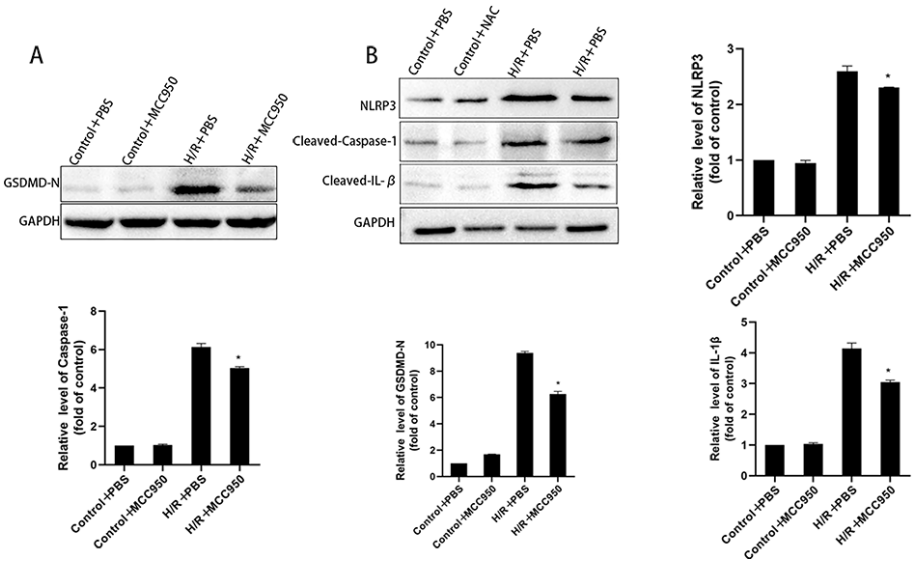

Figure 7. Inhibition of pyroptosis by M2-exos via the ROS/NLRP3 inflammasome pathway. A) Pyroptosis-related proteins in H9c2 cells, were examined by Western blot. B) NLRP3 inflammasome, including NLRP3, cleaved Caspase-1 and IL-1β were examined by Western blot. The values are shown as the mean ± SEM ($N = 6$). *$P < 0.05$ compared with the H/R-PBS group. The experiment was repeated three times.

2014; Ranganathan 2013]. Macrophage-derived exosomes have been revealed to play an immune protective role in inflammatory pain [McDonald 2014]. M2-exos influence the surrounding cells through the paracrine secretion to create the desired environment. Exosomes, nanoparticle extracellular vesicles, possess a phospholipid bilayer membrane and can transport various kinds of contents to recipient cells [Niu 2019; Pant 2012]. RNAs encapsulated in exosomes are particularly stable in body fluids because the RNAs are free from degradation by ribonuclease [Cheng 2019]. During the following phase of inflammation in the MI microenvironment, increasing evidence has revealed the exosomes as mediators denote a key factor in the communication between cardiomyocytes and macrophages [Liu 2020]. Based on the findings from this study, we found that M2-exos also reduced cell death in vitro and in vivo, also found that M2-exos remarkably decreased activation of the NLRP3 inflammasome and of Caspase-1, notably, GSDMD as a major pyroptosis effector was also repressed by M2-exos.

Previous study has reported that sarcoplasmic/endoplasmic reticulum Ca2+-ATPase overexpression may be an effective approach to targeting cardiac microvascular I/R injury by regulating calcium/xanthine oxidase/ROS signaling and preserving mitochondrial quality control [Tan 2020]. Phosphoglycerate mutase 5 also was reported to be involved in driving cardiomyocyte necroptosis through imposing mitochondrial quality control in cardiac I/R injury [Zhu 2021]. Mitochondrial quality control could be a target to delay, reverse, or repair coronary microvascular damage in MI [Chang 2021].

CONCLUSION

In conclusion, very few studies have reported the protective effects of M2 macrophage-derived exosomes in MIR injury. In this study, we evaluated the effects of macrophage-derived exosomes on the development of MI/R injury and further investigated the potential mechanisms underlying focused on suppressing oxidative stress and inflammation to reduce I/R injury. In our present work, we found the activation of NLRP3 inflammasomes and pyroptosis during I/R. More importantly, we discovered that M2-exos have a promising anti-pyroptosis property, which is related to the reduction of NLRP3 inflammasomes.

There also were some limitations in this study. The total mechanisms in regulating myocardial ischemia-reperfusion were still not understood. Moreover, further studies are needed to identify the specific component in the M2-exos.

ACKNOWLEDGEMENT

Funding: This work was supported by the National Natural Science Foundation of China (82070345 and 81870253), Academic promotion program of Shandong First Medical University (2019QL012) and Shandong Taishan Scholarship (Suhua Yan).

REFERENCES

Abderrazak A, Syrovets T, Couchie D, et al. 2015. NLRP3 inflammasome: from a danger signal sensor to a regulatory node of oxidative stress and inflammatory diseases. Redox Biol. 4:296-307.

An N, Gao Y, Si Z, et al. 2019. Regulatory Mechanisms of the NLRP3 Inflammasome, a Novel Immune-Inflammatory Marker in Cardiovascular Diseases. Front Immunol. 10:1592.

Anderson JL, Morrow DA. 2017. Acute Myocardial Infarction. N Engl J Med. 376(21):2053-2064.

Bergsbaken T, Fink SL, Cookson BT. 2009. Pyroptosis: host cell death and inflammation. Nat Rev Microbiol. 7(2):99-109.

Chang X, Lochner A, Wang HH, et al. 2021. Coronary microvascular injury in myocardial infarction: perception and knowledge for mitochondrial quality control. Theranostics. 11(14):6766-6785.

Chen L, Wang Y, Pan Y, et al. 2013. Cardiac progenitor-derived exosomes protect ischemic myocardium from acute ischemia/reperfusion injury. Biochem Biophys Res Commun. 431(3):566-571.

Cheng M, Yang J, Zhao X, et al. 2019. Circulating myocardial microRNAs from infarcted hearts are carried in exosomes and mobilise bone marrow progenitor cells. Nat Commun. 10(1):959.

Cheng Y, Rong J. 2018. Macrophage Polarization as a Therapeutic Target in Myocardial Infarction. Curr Drug Targets. 19(6):651-662.

Denzer K, Kleijmeer MJ, Heijnen HF, Stoorvogel W, Geuze HJ. 2000. Exosome: from internal vesicle of the multivesicular body to intercellular signaling device. J Cell Sci. 113(Pt 19):3365-3374.

Ding J, Wang K, Liu W, et al. 2016. Pore-forming activity and structural autoinhibition of the gasdermin family. Nature. 535(7610):111-116.

Ferdinandy P, Baczkó I, Bencsik P, et al. 2019. Definition of hidden drug cardiotoxicity: paradigm change in cardiac safety testing and its clinical implications. Eur Heart J. 40(22):1771-1777.

Frangogiannis NG. 2015. Inflammation in cardiac injury, repair and regeneration. Curr Opin Cardiol. 30(3):240-245.

Gaspar A, Lourenço AP, Pereira M, et al. 2018. Randomized controlled trial of remote ischaemic conditioning in ST-elevation myocardial infarction as adjuvant to primary angioplasty (RIC-STEMI). Basic Res Cardiol. 113(3):14.

Grivennikov SI, Greten FR, Karin M. 2010. Immunity, inflammation, and cancer. Cell. Mar 19;140(6):883-99.

He Y, Hu H, Wang Y, et al. 2018. ALKBH5 Inhibits Pancreatic Cancer Motility by Decreasing Long Non-Coding RNA KCNK15-AS1 Methylation. Cell Physiol Biochem. 48(2):838-846.

Jung M, Dodsworth M, Thum T. 2018. Inflammatory cells and their non-coding RNAs as targets for treating myocardial infarction. Basic Res Cardiol. 114(1):4.

Kourembanas S. 2015. Exosomes: vehicles of intercellular signaling, biomarkers, and vectors of cell therapy. Annual review of physiology. 77:13-27.

Liu M, Zhou B, Xia ZY, et al. 2013. Hyperglycemia-induced inhibition of DJ-1 expression compromised the effectiveness of ischemic postconditioning cardioprotection in rats. Oxid Med Cell Longev. 2013:564902.

Liu S, Chen J, Shi J, et al. 2020. M1-like macrophage-derived exosomes suppress angiogenesis and exacerbate cardiac dysfunction in a myocardial infarction microenvironment. Basic Res Cardiol. 115(2):22.

Liu X, Zhang Z, Ruan J, et al. 2016. Inflammasome-activated gasdermin D causes pyroptosis by forming membrane pores. Nature. 535(7610):153-158.

Ma Y, Mouton AJ, Lindsey ML. 2018. Cardiac macrophage biology in the steady-state heart, the aging heart, and following myocardial infarction. Transl Res. 191:15-28.

Martinez FO, Gordon S. 2014. The M1 and M2 paradigm of macrophage activation: time for reassessment. F1000Prime Rep. 6:13.

McDonald MK, Tian Y, Qureshi RA, et al. 2014. Functional significance of macrophage-derived exosomes in inflammation and pain. Pain. 155(8):1527-1539.

Merz SF, Korste S, Bornemann L, et al. 2019. Contemporaneous 3D characterization of acute and chronic myocardial I/R injury and response. Nat Commun. 10(1):2312.

Moon BF, Iyer SK, Hwuang E, et al. 2020. Iron imaging in myocardial infarction reperfusion injury. Nat Commun. 11(1):3273.

Niu L, Song X, Wang N, Xue L, Song X, Xie L. 2019. Tumor-derived exosomal proteins as diagnostic biomarkers in non-small cell lung cancer. Cancer Sci. 110(1):433-442.

Pant S, Hilton H, Burczynski ME. 2012. The multifaceted exosome: biogenesis, role in normal and aberrant cellular function, and frontiers for pharmacological and biomarker opportunities. Biochem Pharmacol. 83(11):1484-1494.

Ranganathan PV, Jayakumar C, Ramesh G. 2013. Netrin-1-treated macrophages protect the kidney against ischemia-reperfusion injury and suppress inflammation by inducing M2 polarization. Am J Physiol Renal Physiol. 304(7):F948-F957.

Shi J, Zhao Y, Wang K, et al. 2015. Cleavage of GSDMD by inflammatory caspases determines pyroptotic cell death. Nature. 526(7575):660-665.

Shi J, Zhao Y, Wang Y, et al. 2014. Inflammatory caspases are innate immune receptors for intracellular LPS. Nature. 514(7521):187-192.

Sica A, Allavena P, Mantovani A. 2008. Cancer related inflammation: the macrophage connection. Cancer Lett. 267(2):204-215.

Tan Y, Mui D, Toan S, et al. 2020. SERCA Overexpression Improves Mitochondrial Quality Control and Attenuates Cardiac Microvascular Ischemia-Reperfusion Injury. Mol Ther Nucleic Acids. 22:696-707.

Teng X, Chen L, Chen W, Yang J, Yang Z, Shen Z. 2015. Mesenchymal Stem Cell-Derived Exosomes Improve the Microenvironment of Infarcted Myocardium Contributing to Angiogenesis and Anti-Inflammation. Cell Physiol Biochem. 37(6):2415-2424.

van der Vorst EPC, Weber C. 2019. Novel Features of Monocytes and Macrophages in Cardiovascular Biology and Disease. Arterioscler Thromb Vasc Biol. 39(2):e30-e37.

Vicencio JM, Yellon DM, Sivaraman V, et al. 2015. Plasma exosomes protect the myocardium from ischemia-reperfusion injury. J Am Coll Cardiol. 65(15):1525-1536.

Wang Y, Chen Q, Jiao F, et al. 2021. Histone deacetylase 2 regulates ULK1 mediated pyroptosis during acute liver failure by the K68 acetylation site. Cell Death Dis. 12(1):55.

Wrobel K, Stevens SR, Jones RH, et al. 2015. Influence of Baseline Characteristics, Operative Conduct, and Postoperative Course on 30-Day Outcomes of Coronary Artery Bypass Grafting Among Patients With Left Ventricular Dysfunction: Results From the Surgical Treatment for Ischemic Heart Failure (STICH) Trial. Circulation. 132(8):720-730.

Xiao B, Chai Y, Lv S, et al. 2017. Endothelial cell-derived exosomes protect SH-SY5Y nerve cells against ischemia/reperfusion injury. Int J Mol Med. 40(4):1201-1209.

Xiong Y, Chen L, Yan C, et al. 2020. M2 Macrophagy-derived exosomal miRNA-5106 induces bone mesenchymal stem cells towards osteoblastic fate by targeting salt-inducible kinase 2 and 3. J Nanobiotechnology. 18(1):66.

Xu R, Rai A, Chen M, Suwakulsiri W, Greening DW, Simpson RJ. 2018. Extracellular vesicles in cancer - implications for future improvements in cancer care. Nat Rev Clin Oncol. 15(10):617-638.

Xue R, Lei S, Xia ZY, et al. 2016. Selective inhibition of PTEN preserves ischaemic post-conditioning cardioprotection in STZ-induced Type 1 diabetic rats: role of the PI3K/Akt and JAK2/STAT3 pathways. Clin Sci (Lond).130(5):377-392.

Yue S, Rao J, Zhu J, et al. 2014. Myeloid PTEN deficiency protects livers from ischemia reperfusion injury by facilitating M2 macrophage differentiation. J Immunol. 192(11):5343-5353.

Zhang ZG, Buller B, Chopp M. 2019. Exosomes - beyond stem cells for restorative therapy in stroke and neurological injury. Nat Rev Neurol. 15(4):193-203.

Zhu H, Tan Y, Du W, et al. 2021. Phosphoglycerate mutase 5 exacerbates cardiac ischemia-reperfusion injury through disrupting mitochondrial quality control. Redox Biol. 38:101777.